Water Splitting

International Edition: DOI: 10.1002/anie.201502438
German Edition: DOI: 10.1002/ange.201502438

The Synthesis of Nanostructured Ni_5P_4 Films and their Use as a Non-Noble Bifunctional Electrocatalyst for Full Water Splitting**

*Marc Ledendecker, Sandra Krick Calderón, Christian Papp, Hans-Peter Steinrück, Markus Antonietti, and Menny Shalom**

Abstract: *The investigation of nickel phosphide (Ni_5P_4) as a catalyst for the hydrogen (HER) and oxygen evolution reaction (OER) in strong acidic and alkaline environment is described. The catalyst can be grown in a 3D hierarchical structure directly on a nickel substrate, thus making it an ideal candidate for practical water splitting devices. The activity of the catalyst towards the HER, together with its high stability especially in acidic solution, makes it one of the best non-noble materials described to date. Furthermore, Ni_5P_4 was investigated in the OER and showed activity superior to pristine nickel or platinum. The practical relevance of Ni_5P_4 as a bifunctional catalyst for the overall water splitting reaction was demonstrated, with 10 mA cm^{-2} achieved below 1.7 V.*

The availability of peak excess electricity from wind and solar energy makes temporal storage in high-energy chemicals a mandatory task for chemistry. Here, the focus lies especially on hydrogen which can be "easily" electrolyzed from water, then effectively reconverted into electricity with a number of available devices.[1] Although electrolysis of water into hydrogen and oxygen is considered to be one of the easiest and cleanest methods to obtain hydrogen, this reaction is far from optimized. Currently, the reaction still requires high overpotentials for both the hydrogen (HER) and oxygen evolution reaction (OER) to obtain decent reaction rates. For example, around 50% (1.8–2 V instead of 1.23 V) excess potential is required in industrial electrolyzer cells, which account for less than 5% of the world production of hydrogen.[2] This excess potential already represents an energy penalty of at least 35% in the first conversion step, which makes it less attractive for an energy storage scheme. In addition, common electrolyzers are based on rare noble metals, such as Pt alloys for hydrogen evolution and IrO_2/RuO_2 for oxygen evolution, and a broader distribution of such devices stays rather questionable.

[*] M. Ledendecker, Prof. Dr. M. Antonietti, Dr. M. Shalom
Max Planck Institute of Colloids and Interfaces
Am Mühlenberg 1, 14476 Potsdam (Germany)
E-mail: Menny.Shalom@mpikg.mpg.de
S. Krick Calderón, Dr. C. Papp, Prof. Dr. H.-P. Steinrück
Department of Physical Chemistry II
Friedrich-Alexander Universität Erlangen Nürnberg
Egerlandstrasse 3, 91058 Erlangen (Germany)

[**] S.K.C., C.P., and H.-P.S. greatly acknowledge support by the Cluster of Excellence Engineering of Advanced Materials (EAM) at the Friedrich-Alexander-University Erlangen-Nürnberg.

Supporting information for this article is available on the WWW under http://dx.doi.org/10.1002/anie.201502438.

The OER is considered to be the bottle-neck in the water splitting reaction as a result of the multielectron transfer reaction being sluggish.[3] Usually, onset overpotentials of over 300 mV are needed when using approaches based on non-noble metals (mostly 3d transition metals).[4] Up to now, ample research has been dedicated towards nickel and its oxides (nickel hydroxides and nickel oxyhydroxides) and their role in the HER and OER, but investigations of ceramic Ni materials (phosphides, nitrides, or carbides) as OER catalysts or even as bifunctional catalysts (capable of catalyzing in this case both reaction sides) are still limited.[5] Recently, nickel sulfide, which has traditionally been used for the HER, displayed promising activity also as an OER catalyst, with NiSOH proposed to be the active species.[6]

Therefore, it is still necessary to find more efficient electrocatalysts which are based on earth-abundant materials. Among these materials, metal phosphides such as FeP,[7] Ni_2P,[8] $Ni_{12}P_5$,[9] CoP_2,[10] CoP,[11] and Mo_3P[12] have indeed already shown great potential as HER catalysts, with stable behavior in acid as well as in base and high current densities at low overpotentials. The high activity of metal phosphides was attributed to the phosphorus in the structure being able to take part in the reaction through moderate bonding to the reaction intermediates, thereby creating a surface with proton acceptor and hydride acceptor sites.[13] Among this group, very recently, Ni_5P_4 particles were also reported as efficient HER catalysts, with high performance in acidic and basic media.[14] Most of these catalyst preparations are based on nanoparticles that show a high surface area, but also have some disadvantages such as uncontrolled agglomeration, higher series resistances, still-existing templates, and easier oxidation. Here, we strive for an easy and straightforward synthesis of the catalyst directly on the current collector, which then allows direct use in devices, that is, for electrolyzers, as cathodes in solar cells and for artificial leaves.[15] The possibility of synthesizing the catalyst directly on the current collector received not only attention in catalysis (Ni_2P foam,[16] CoP[17]) but also as electrodes, for example, in supercapacitors.[18]

Here we show a simple method to synthesize highly ordered Ni_5P_4 nanoarchitectures directly on Ni foil. Ni_5P_4 grows perpendicular to the surface and exhibits "disklike" morphology with preferentially exposed faces. The bifunctional electrocatalytic activity of this Ni_5P_4 nanostructure towards both the HER and OER, with competitive performances in both reactions, is demonstrated. The composition, morphology, and surface of the catalyst was studied by scanning electron microscopy (SEM), transmission electron microscopy (TEM), selected-area electron diffraction

(SAED) energy-dispersive X-ray spectroscopy (EDX), infrared (IR) and Raman spectroscopy, X-ray diffraction (XRD), and X-ray photoelectron spectroscopy (XPS). For electrochemical characterizations, cyclic voltammetry (CV), linear-sweep voltammetry (LSV), chronoamperometric measurements (CA), electrochemical impedance spectroscopy (EIS), and chronopotentiometric (CP) techniques were utilized. To complement the results gained, inductively coupled plasma optical emission spectrometry (ICP-OES) and oxygen probe measurements were performed.

Ni_5P_4 was prepared by simple heating of nickel foil and red phosphorus for 1 h at 550 °C under an inert atmosphere in a typical contact-conversion synthesis. Contamination by other elements could be excluded by using only elemental phosphorus and nickel as precursors. The formation of Ni_5P_4 was monitored by SEM at different time intervals (Figure S1). First, adsorption of phosphorus onto the metal surface took place, which was followed by the formation of a thin film after less than 10 min heating time. After one hour, the film thickness was approximately 40 μm and was proven to be composed of phosphorus/nickel (Figure 1 c). This means that during growth, phosphorus ions are able to diffuse through the nickel phosphide material (the full EDX spectrum is presented in Figure S2).

Figure 1 a shows the XRD pattern of the experimentally obtained Ni_5P_4-modified nickel foil and the reference pattern. The peak positions of Ni_5P_4 were in very good agreement with the experimental data, even though the directed growth of Ni_5P_4 (Figure 1 b) led to increased relative peak intensities deviating from the reference sample. The SEM images of the as-received and the modified nickel foil are displayed in Figure 1 b (see also Figure S1 and Figure S3). The as-received nickel foil shows the characteristic striation pattern from its fabrication process, while sheet formation of Ni_5P_4 perpendicular to the surface was observed after modification, thus agreeing with the observation by XRD of directed growth. The mean nickel to phosphorus ratio determined by EDX mapping from eight different Ni_5P_4 samples (same synthesis route) and measured by ICP-OES coincide appropriately to the theoretical value of Ni_5P_4 ($Ni/P_{EDX} = 1.32$, $Ni/P_{ICP} = 1.16$, $Ni/P_{theo} = 1.25$). SAED patterns and TEM images accentuates the high degree of crystallinity, thus excluding other crystalline side products (Figure 1 d).

The surface composition of the Ni_5P_4 sample was studied by ex situ XPS measurements (Figure S4). The full interpretation of the XPS data can be found in the Supporting Information. The signal at 857.5 eV with a satellite at 862.6 eV in the Ni 2p region in the spectra after synthesis is assigned to nickel phosphate. Peaks for two chemical species are found in the P 2p region at 130.0 and 134.1 eV, which are assigned to phosphide and phosphate signals. In addition, spectra were recorded after heating the samples to 1000 K for 10 min in an ultrahigh vacuum to reduce impurities on the surface arising from exposure to ambient conditions. In the Ni 2p region, a peak at 853.6 eV with a satellite at 859.7 eV is observed, which is assigned to phosphidic or metallic nickel.[19] These assignments are in line with previous results of a Ni-P alloy showing a binding energy of 853.0 eV for nickel phosphide and 857.5 eV for nickel phosphate.[20] Interestingly, both oxidation states of phosphorus are still observed in the P 2p region. This is explained by different information depths of the Ni 2p and P 2p core levels; while the Ni 2p core level is sensitive to the surface, due to the larger inelastic mean free path at the higher kinetic energy of the electrons, the P 2p region is also sensitive to the bulk. The reduction of nickel is in line with the change in the relative amounts of phosphide and phosphate in the P 2p region: the fact that more phosphide is present after heating to 1000 K shows that the phosphate is (partly) removed by heating to 1000 K, thus allowing the identification of NiP on the surface.

The catalytic activity towards the HER of Ni_5P_4 was evaluated by sweeping from a positive to a negative potential (from 0.1 V to −0.5 V versus RHE) in a three-electrode setup (see the Supporting Information) and was compared to Pt and Ni. The catalysts were evaluated in 0.5 M H_2SO_4 and 1 M KOH while rotating the electrode at 2000 rpm to minimize mass transport limitations (Figure 2). The performance of Ni_5P_4 in acid (overpotential of ca. 0.14 V at $-10\ mA\,cm^{-2}$) and in base (ca. 0.15 V at $-10\ mA\,cm^{-2}$) greatly outperformed that of nickel (0.21 V in base, not stable in acid) and is one of highest non-noble metal catalysts, but the performance is not as good as platinum foil (ca. 0.05 V at $-10\ mA\,cm^{-2}$ in acid, ca. 0.09 V at $-10\ mA\,cm^{-2}$ in base; for comparison, selected state of the

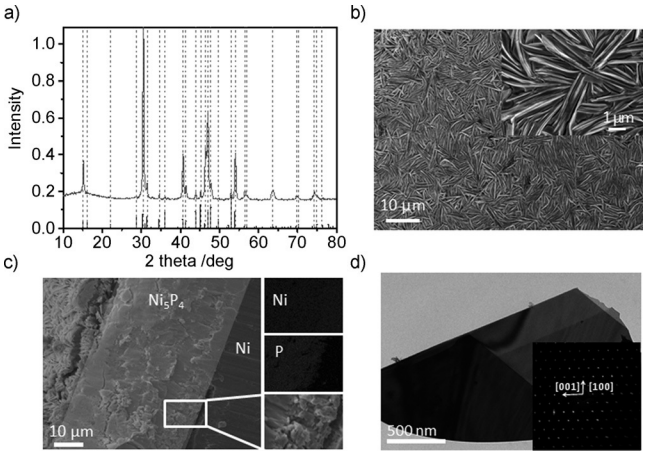

Figure 1. Material characteristics for Ni_5P_4: a) experimentally obtained XRD pattern and reference pattern of Ni_5P_4 (ICDD 04-014-7901). b) Top view and c) cross-section SEM images of Ni_5P_4 (rectangle) on nickel foil and the corresponding element distributions by EDX. d) TEM/SAED image of Ni_5P_4 scratched off the surface.

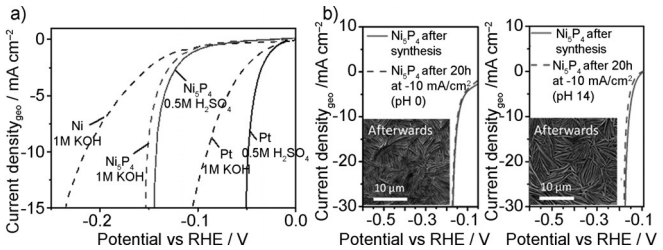

Figure 2. a) Hydrogen evolution reaction of Pt, Ni_5P_4, and pristine nickel foil at pH 0 (straight line) and pH 14. b) Long-term stability measurement of Ni_5P_4 in 1 M KOH and 0.5 M H_2SO_4 for a 20 h period and the corresponding SEM images after testing.

art catalysts towards the HER can be found in Table S1).[8,21] The electrode kinetics of Ni_5P_4 were studied using chronoamperomerty measurements by scanning from positive to negative potentials in 10 mV steps [60 s each step; the resulting Tafel plots (log(current density) versus overpotential) for Ni_5P_4, Pt, and Ni in alkaline and acid solutions are displayed in Figure S5].

Tafel slopes of approximately 53 mV dec^{-1} in alkaline and 40 mV dec^{-1} in acidic solution were found for Ni_5P_4, thus indicating a Volmer–Heyrovsky mechanism. Platinum and nickel show the expected Tafel slopes of approximately 32 and 121 mV dec^{-1}, respectively, thus indicating the Tafel and Volmer step to be rate-determining.[22] A more detailed discussion can be found in the Supporting Information. Stability plays a major role in water splitting devices because of the direct correlation of the lifetime of the catalyst and the cost of hydrogen. Therefore, long-term stability tests (Figure 2b) were performed at pH 0 and pH 14 in a three-electrode setup. Thereby, linear-sweep voltammetry (LSV) curves were recorded before and after keeping the current density at -10 mA cm^{-2} for 20 h while monitoring the voltage changes (Figure S6). Ni_5P_4 showed high stability during the 20-hour test, especially in acidic solution, with no clear change in morphology as demonstrated by SEM imaging. Furthermore, no change in crystallinity could be observed by XRD after the respective tests (Figure S7). Despite the high electrochemical stability of the Ni_5P_4 material, recent studies by Chorkendorff and co-workers showed that electrochemical stability is not enough to appraise the total stability of the material, as partial dissolution of the electrocatalyst must also be excluded.[23] To confirm the total stability, nickel dissolution was monitored with ICP-OES during electrochemical stability measurements over a 20 h time period (Figure S8). After 20 h, a relatively small amount (520 μg) of Ni was found in solution. Furthermore ex situ XPS was recorded after the HER stability measurements both in acid and in alkaline medium. For pristine nickel, it is known that a thin layer of $Ni(OH)_2$ is always present at an open circuit potential in alkaline medium.[24] Interestingly, after HER in 1 M KOH, $Ni(OH)_2$ might also form on the Ni_5P_4 surface. In the Ni 2$p_{3/2}$ region, the dominating signal at approximately 857 eV is shifted about 3.5 eV relative to metallic nickel and no signal in the P 2p region is observed (Figures S9 and S10), which supports this argument.[25] Nickel phosphide peaks emerge in the Ni 2$p_{2/3}$ (853.6 eV) and in the P 2p region after heating the samples to 1000 K for 10 min in an ultrahigh vacuum. In contrast, phosphate peaks in the P 2p region were observed after stability tests in 0.5 M H_2SO_4 (Figure S11). The formation of a protective nickel phosphate layer might prevent dissolution of the nickel phosphide by acting as a diffusion barrier, and might be one reason for the observed stability of Ni_5P_4 in acid.[20,26] Again, the phosphidic nature of the material was restored after heating, thus indicating the reversibility of the oxygen binding onto the surface. A high surface area of the active catalyst is required for real application purposes (e.g. electrolyzer cells). To obtain higher surface areas, Ni_5P_4 was synthesized directly on nickel foam instead of nickel foil (Figure S12). As a consequence of the higher surface area, the current density increased drastically up to 100 mA cm^{-2} at 0.17 V overpotential. However, we note that because of the complete conversion of metallic Ni into Ni_5P_4, the foam slightly lost its flexibility, thus making it more difficult to handle. The performance of Ni_5P_4 towards the oxygen evolution reaction (OER) was explored in alkaline media. In general, the most active non-noble metal (Ni, Fe, Co) based catalysts for the OER are metal oxyhydroxides (MOOH). Pristine nickel converts into nickel hydroxide and oxyhydroxide during the oxidation of water, where the first step entails the formation of $Ni(OH)_2$,[27] which can be converted reversibly into NiOOH at higher potentials ($E >$ 1.53 V versus RHE).[28] However, the electrochemical formation of highly active NiOOH is still low for pristine Ni. Consequently, new synthesis methods are desired to obtain supported, catalytically active NiOOH as an efficient OER catalyst.[29] Cyclic voltammetry curves of Ni_5P_4, Ni, and Pt are shown in Figure 3a. When examining the oxygen evolution reaction for all three materials, it is evident that Ni_5P_4 performs the best, with a high current density at low overpotentials compared to nickel and platinum (a comparison of other state of the art OER catalysts is given in Table S2). As predicted by the Bode diagram, NiOOH formation preceded the OER reaction, and acts as the active catalyst in the OER.[30] After NiOOH formation, the back reduction to $Ni(OH)_2$ could be observed at around 1.25 V versus RHE. Without any activation treatment or aging beforehand, the stability of Ni_5P_4 and Ni in the OER was compared by keeping the current density constant at 10 mA cm^{-2} over a 20 h time period (Figure 3b). In this very simple procedure, a lower overpotential at the same current density was achieved with Ni_5P_4 compared to pristine Ni, accompanied by higher long-term stability (the Tafel analysis

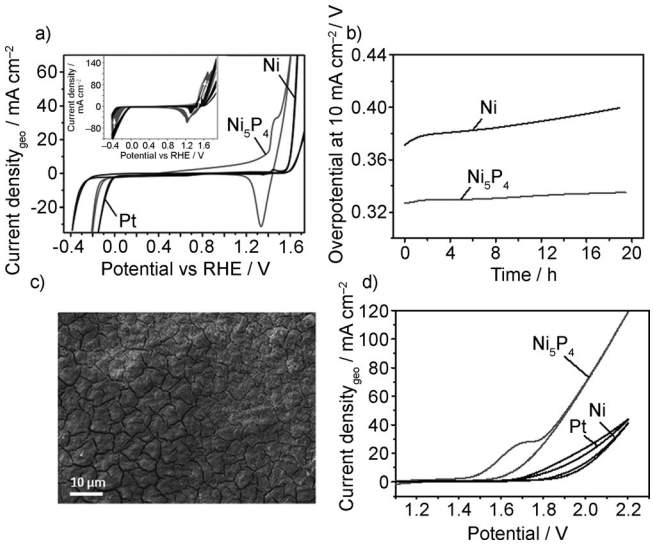

Figure 3. a) First electrochemical cycle of Ni, Pt, and Ni_5P_4 in 1 M KOH using a scan rate of 40 mV s^{-1} and rotation at 2000 rpm (iR corrected). The inset shows the change in material during electrochemical aging (500 cycles). b) Oxygen evolution reaction of Ni and Ni_5P_4 at pH 14 without electrochemical pretreatment at 10 mA cm^{-2} (iR corrected). c) The morphology of Ni_5P_4 after 500 cycles by SEM imaging. d) Different catalysts (Ni_5P_4, Ni, and Pt) tested in a two-electrode setup for the overall water-splitting reaction in 1 M KOH (not iR corrected).

of Ni_5P_4 for the oxygen evolution reaction in 1M KOH is shown in Figure S13, which shows a Tafel slope of ca. 40 mV dec^{-1} that is characteristic for NiOOH;[31] the full discussion can be found in the Supporting information). The superior activity of Ni_5P_4 as an electrocatalyst in the OER can be attributed to several factors. Catalytically active NiOOH can be easily formed on top of Ni_5P_4 presumably as a result of the unique "sheetlike" morphology. Furthermore, it is well known that the substrate has a strong influence on the performance of the (electro)catalyst because of alterations to the electronic properties.[32] In this manner, the formation of a Ni_5P_4/NiOOH heterojunction ("supported NiOOH") can enhance the electronic configuration, thereby leading to a lower overpotential with a higher current density in the OER, but explaining also the significantly higher stability of the catalytic system.

Most work in the literature determines the onset potential for the OER by simple extrapolation of the current voltage curves. However, as a consequence of the preceding and overlapping formation of NiOOH at low overpotenials, in our case it was easy to make mistakes. Therefore, the amount of oxygen was carefully monitored with an optical oxygen probe coupled in a typical three-electrode setup. An onset overpotential of 0.25 V, which is similar to that of noble metals, was measured using chronoamperometry measurements in 5 mV steps (each step 60 s) for the oxygen evolution region while monitoring the oxygen content in solution (Figure S14).

To further understand the system at hand, accelerated electrochemical aging (electrochemical cycling between −0.43 V and 1.75 V versus RHE, 500 times) of Ni, Ni_5P_4, and Pt was performed. The performance of both Ni_5P_4 and Ni increased (Figure 3a, inset). After cycling, the surface of Ni_5P_4 adopted a cracked morphology (Figure 3c). The XRD pattern after aging and one additional scan to 1.6 V (NiOOH is formed) showed that there is still underlying Ni_5P_4 present, thus implying that the formed NiOOH is amorphous and supported (Figure S7).[24] The EDX mapping of the electrode cross-section after electrochemical aging revealed that the first few micrometers consist of nickel and oxygen while nickel and phosphorus (Ni_5P_4) can be found underneath (Figure S15). Further evidence in favor of the successful formation of a Ni_5P_4/NiOOH heterojunction was provided by FTIR (Figure S16) and ICP-OES (Figure S17) measurements on the solution after electrochemical aging. During cycling, not only was nickel oxidized, but so was the phosphorus counterpart, thereby resulting in pronounced phosphate peaks in solution. Additional proof of the formation of higher oxides (apart from electrochemical characterization) was provided by ex situ Raman spectroscopy (Figure S18) showing two peaks at 470 cm^{-1} and 550 cm^{-1}, which were assigned as Ni-O bending and stretching vibrations corresponding to active NiOOH.[28]

To illustrate practical relevance, the overall water splitting reaction was investigated in a two-electrode setup using the same material as cathode and anode (Figure 3d) in an alkaline environment (pH 14). In this case, 10 mA cm^{-2} could be achieved by applying less than 1.7 V between the two electrodes for Ni_5P_4 compared to over 1.8 V for Pt and over 1.9 V for pristine Ni. This translates into 72% efficiency under those very simple conditions and enables use, for example, in photovoltaics.[33]

In summary, a straightforward synthesis of highly ordered Ni_5P_4 sheets grown directly on a current collector was presented. The as-prepared Ni_5P_4/Ni foil exhibits low overpotential along with high stability in acidic and in alkaline media for the HER. The 3D hierarchical architecture favors the facile formation of catalytically active NiOOH on Ni_5P_4 as a result of the easy replacement of phosphorus in the form of phosphates in solution. The high activity as well as stability illustrates the significant importance of the substrate by forming a Ni_5P_4/NiOOH heterojunction and altering thereby the electronic properties towards lower OER overpotentials. These beneficial effects, which lead to low onset potentials in the hydrogen and oxygen evolution, accompanied by the simple synthesis involving earth-abundant materials further underlines the promising potential of nickel phosphides towards the full electrocatalytic splitting reaction of water.

Keywords: ceramics · hydrogen evolution reaction · nickel phosphides · oxygen evolution reaction · water splitting reaction

How to cite: *Angew. Chem. Int. Ed.* **2015**, *54*, 12361–12365
Angew. Chem. **2015**, *127*, 12538–12542

[1] T. E. Mallouk, *Nat. Chem.* **2013**, *5*, 362–363.
[2] a) S. Dunn, *Int. J. Hydrogen Energy* **2002**, *27*, 235–264; b) R. F. de Souza, J. C. Padilha, R. S. Gonçalves, M. O. de Souza, J. Rault-Berthelot, *J. Power Sources* **2007**, *164*, 792–798; c) K. Zeng, D. Zhang, *Prog. Energy Combust. Sci.* **2010**, *36*, 307–326.
[3] a) M. Gattrell, B. MacDougall in *Handbook of Fuel Cells*, Wiley, Hoboken, **2010**; b) C. Zhang, M. Antonietti, T.-P. Fellinger, *Adv. Funct. Mater.* **2014**, *24*, 7655–7665.
[4] a) R. Subbaraman, D. Tripkovic, K.-C. Chang, D. Strmcnik, A. P. Paulikas, P. Hirunsit, M. Chan, J. Greeley, V. Stamenkovic, N. M. Markovic, *Nat. Mater.* **2012**, *11*, 550–557; b) C. C. L. McCrory, S. Jung, J. C. Peters, T. F. Jaramillo, *J. Am. Chem. Soc.* **2013**, *135*, 16977–16987; c) M. Ledendecker, G. Clavel, M. Antonietti, M. Shalom, *Adv. Funct. Mater.* **2015**, *25*, 393–399.
[5] M. Shalom, D. Ressnig, X. Yang, G. Clavel, T. P. Fellinger, M. Antonietti, *J. Mater. Chem. A.* **2015**, *25*, 8171–8177.
[6] W. Zhou, X.-J. Wu, X. Cao, X. Huang, C. Tan, J. Tian, H. Liu, J. Wang, H. Zhang, *Energy Environ. Sci.* **2013**, *6*, 2921–2924.
[7] P. Jiang, Q. Liu, Y. Liang, J. Tian, A. M. Asiri, X. Sun, *Angew. Chem. Int. Ed.* **2014**, *53*, 12855–12859; *Angew. Chem.* **2014**, *126*, 13069–13073.
[8] E. J. Popczun, J. R. McKone, C. G. Read, A. J. Biacchi, A. M. Wiltrout, N. S. Lewis, R. E. Schaak, *J. Am. Chem. Soc.* **2013**, *135*, 9267–9270.
[9] Z. Huang, Z. Chen, Z. Chen, C. Lv, H. Meng, C. Zhang, *ACS Nano* **2014**, *8*, 8121–8129.
[10] A. Lu, Y. Chen, H. Li, A. Dowd, M. B. Cortie, Q. Xie, H. Guo, Q. Qi, D.-L. Peng, *Int. J. Hydrogen Energy* **2014**, *39*, 18919–18928.
[11] a) E. J. Popczun, C. G. Read, C. W. Roske, N. S. Lewis, R. E. Schaak, *Angew. Chem. Int. Ed.* **2014**, *53*, 5427–5430; *Angew. Chem.* **2014**, *126*, 5531–5534; b) Q. Liu, J. Tian, W. Cui, P. Jiang, N. Cheng, A. M. Asiri, X. Sun, *Angew. Chem. Int. Ed.* **2014**, *53*, 6710–6714; *Angew. Chem.* **2014**, *126*, 6828–6832.
[12] P. Xiao, M. A. Sk, L. Thia, X. Ge, R. J. Lim, J.-Y. Wang, K. H. Lim, X. Wang, *Energy Environ. Sci.* **2014**, *7*, 2624–2629.
[13] P. Liu, J. A. Rodriguez, *J. Am. Chem. Soc.* **2005**, *127*, 14871–14878.

[14] A. B. Laursen, K. R. Patraju, M. J. Whitaker, M. Retuerto, T. Sarkar, N. Yao, K. V. Ramanujachary, M. Greenblatt, G. C. Dismukes, *Energy Environ. Sci.* **2015**, *8*, 1027 – 1034.
[15] a) K. Sun, X. Pang, S. Shen, X. Qian, J. S. Cheung, D. Wang, *Nano Lett.* **2013**, *13*, 2064 – 2072; b) M. J. Kenney, M. Gong, Y. Li, J. Z. Wu, J. Feng, M. Lanza, H. Dai, *Science* **2013**, *342*, 836 – 840; c) M. S. Faber, K. Park, M. Cabán-Acevedo, P. K. Santra, S. Jin, *J. Phys. Chem.* **2013**, *4*, 1843 – 1849.
[16] a) X. Wang, Y. V. Kolen'ko, L. Liu, *Chem. Commun.* **2015**, *51*, 6738 – 6741; b) Y. Shi, Y. Xu, S. Zhuo, J. Zhang, B. Zhang, *ACS Appl. Mater. Interfaces* **2015**, *7*, 2376 – 2384.
[17] a) Y. Yang, H. Fei, G. Ruan, J. M. Tour, *Adv. Mater.* **2015**, *27*, 3174 – 31800; b) N. Jiang, B. You, M. Sheng, Y. Sun, *Angew. Chem. Int. Ed.* **2015**, *54*, 6251 – 6254; *Angew. Chem.* **2015**, *127*, 6349 – 6352; c) J. Tian, Q. Liu, A. M. Asiri, X. Sun, *J. Am. Chem. Soc.* **2014**, *136*, 7587 – 7590.
[18] R. Madhu, V. Veeramani, S.-M. Chen, P. Veerakumar, S.-B. Liu, *Chem. Eur. J.* **2015**, *21*, 8200 – 82060.
[19] R. Franke, *Spectrochim. Acta* **1997**, *53*, 933 – 941.
[20] B. Elsener, M. Crobu, M. Scorciapino, A. Rossi, *J. Appl. Electrochem.* **2008**, *38*, 1053 – 1060.
[21] a) L. Feng, H. Vrubel, M. Bensimon, X. Hu, *Phys. Chem. Chem. Phys.* **2014**, *16*, 5917 – 5921; b) W. F. Chen, C. H. Wang, K. Sasaki, N. Marinkovic, W. Xu, J. T. Muckerman, Y. Zhu, R. R. Adzic, *Energy Environ. Sci.* **2013**, *6*, 943 – 951; c) J. R. McKone, B. F. Sadtler, C. A. Werlang, N. S. Lewis, H. B. Gray, *ACS Catal.* **2012**, *2*, 166 – 169.
[22] J. Barber, S. Morin, B. E. Conway, *J. Electroanal. Chem.* **1998**, *446*, 125 – 138.
[23] R. Frydendal, E. A. Paoli, B. P. Knudsen, B. Wickman, P. Malacrida, I. E. L. Stephens, I. Chorkendorff, *ChemElectroChem* **2014**, *1*, 2075 – 2081.
[24] C. Bocca, A. Barbucci, G. Cerisola, *Int. J. Hydrogen Energy* **1998**, *23*, 247 – 252.
[25] D. S. Hall, C. Bock, B. R. MacDougall, *J. Electrochem. Soc.* **2013**, *160*, F235 – F243.
[26] A. R. J. Kucernak, V. N. Naranammalpuram Sundaram, *J. Mater. Chem.* **2014**, *2*, 17435 – 17445.
[27] S. Deabate, F. Henn, *Electrochim. Acta* **2005**, *50*, 2823 – 2835.
[28] J. McBreen, *Handbook of Battery Materials*, Wiley-VCH, Weinheim, **2007**, pp. 135 – 151.
[29] H.-Y. Wang, Y.-Y. Hsu, R. Chen, T.-S. Chan, H. M. Chen, B. Liu, *Adv. Energy Mater.* **2015**, *5*.
[30] P. W. T. Lu, S. Srinivasan, *J. Electrochem. Soc.* **1978**, *125*, 1416 – 1422.
[31] M. W. Louie, A. T. Bell, *J. Am. Chem. Soc.* **2013**, *135*, 12329 – 12337.
[32] a) V. Molinari, C. Giordano, M. Antonietti, D. Esposito, *J. Am. Chem. Soc.* **2014**, *136*, 1758 – 1761; b) X.-H. Li, M. Antonietti, *Chem. Soc. Rev.* **2013**, *42*, 6593 – 6604.
[33] J. Luo, J.-H. Im, M. T. Mayer, M. Schreier, M. K. Nazeeruddin, N.-G. Park, S. D. Tilley, H. J. Fan, M. Grätzel, *Science* **2014**, *345*, 1593 – 1596.

Received: March 17, 2015
Published online: June 30, 2015

